Carbohydrate Polymers 110 (2014) 87–94

Contents lists available at ScienceDirect

Carbohydrate Polymers

journal homepage: www.elsevier.com/locate/carbpol

In situ hydrogel constructed by starch-based nanoparticles via a Schiff base reaction

Yangling Li[a,b], Chang Liu[a,b], Ying Tan[a,*], Kun Xu[a], Cuige Lu[a,b], Pixin Wang[a,*]

[a] Key Laboratory of Polymer Ecomaterials, Changchun Institute of Applied Chemistry, Chinese Academy of Science, 130022, PR China
[b] Graduate University of Chinese Academy of Sciences, Beijing 100049, PR China

ARTICLE INFO

Article history:
Received 28 November 2013
Received in revised form 17 March 2014
Accepted 22 March 2014
Available online 30 March 2014

Keywords:
Hydrogel
In situ
Schiff base
Starch
Nanoparticles

ABSTRACT

Polysaccharide-based hydrogels are remarkable materials for the biomedical fields because of its excellent biodegradation and biocompatibility. In this work, a novel polysaccharide-based hydrogel was fabricated by in situ crosslinking of starch-based nanoparticles and polyvinylamine. Starch was decorated with cholesterol group and aldehyde groups. TEM and DLS showed that the cholesterol modified oxidation starch (OCS) exhibited a core–shell nanoparticles with mean size of ~143 nm in aqueous. The hydrogel was then synthesized via Schiff base reaction. Rheological measurements demonstrated the incorporation of cholesterol groups not only reduced the gel time but also improved the storage modulus of the hydrogel compared with the oxide starch crosslinked hydrogel. SEM showed the OCS based hydrogels possess a well-defined porous structure. Furthermore, doxorubicin (DOX) was used as model drug to investigate the control and release properties of OCS hydrogels. This OCS hydrogel would be a promising drug carrier for biomedical applications.

1. Introduction

Hydrogel, as a hydrophilic polymer network with amounts of water, has been a promising material for biomedical applications because of its flexibility which was similar to soft tissue (Kiyonaka et al., 2004; Nowak et al., 2002; Seliktar, 2012). Hydrogel can be derivated from natural and synthetic polymers. The natural polymers are usually biocompatibility and biodegradation that do not produce adverse reproductive and developmental effects (Chiu et al., 2009; Ding et al., 2012; Wang, Cui, Li, & van Hest, 2012). So the hydrogel based on natural materials are being investigated for drug/protein delivery (Qiu & Park, 2012; Tokarev & Minko, 2010), tissue engineering (Boucard, Viton, & Domard, 2005; Yu et al., 2014) and biosensors (Park, Jang, Koh, & Kim, 2010; Sugaya, Kakegawa, Fukushima, Yamada, & Seki, 2012).

In situ forming hydrogels are preferable for biomedical applications because they can be deployed by injection instead of surgical implantation. Generally, in situ hydrogels can be synthesized via physical or chemical approach (Censi, Fieten, di Martino, Hennink, & Vermonden, 2010; Palumbo et al., 2012). Compare to physical pattern, the chemical approach may produce hydrogel with a higher mechanical strength. The typical in situ chemical approach includes Schiff base reactions (Weng et al., 2013; Zhang, Qadeer, & Chen, 2011), Michael addition reactions (Censi et al., 2010; Peng et al., 2013; Wang, Zong, Zhao, Zhuo, & Cheng, 2011), ionic interactions (Li & Mezzenga, 2012; Tomme, van Steenbergen, De Smedt, van Nostrum, & Hennink, 2005; Yang & Urban, 2013) or photo-crosslinking reactions (Fan, Deng, Cheng, Meng, & Zhong, 2013).

Schiff base is synthesized from amine and carbonyl groups by nucleophilic addition to generate an imine group. It is biodegradable via hydrolysis, and the stability of these bonds decreases as the pH decreasing. So it is very suitable for use in the field of biomedical and tissue engineering. Saito, Hoffman, and Ogawa (2007) have prepared a PEG hydrogel based on Schiff base reaction to delivery doxorubicin (DOX). The result shows that this hydrogel is a good drug carrier for DOX. Similarly, Nair, Remya, Remya, and Nair (2011) have reported an injectable hydrogel based on Schiff base for tissue engineering applications. The fibroblast cells seeded onto the hydrogel scaffolds could be adhered, proliferated and produced ECM components on the scaffold. Likewise, chondrocytes encapsulated in hydrogels retained their viability and specific phenotypic characteristics.

Starch is a natural carbohydrate consists of two major components: amylose and amylopectin. Amylose is a primarily linear polysaccharide with α-(1–4)-linked D-glucose units, while

* Corresponding authors. Tel.: +86 431 85262622; fax: +86 431 85262629.
E-mail addresses: tanying@ciac.ac.cn (Y. Tan), pxwang@ciac.ac.cn (P. Wang).

http://dx.doi.org/10.1016/j.carbpol.2014.03.058
0144-8617/

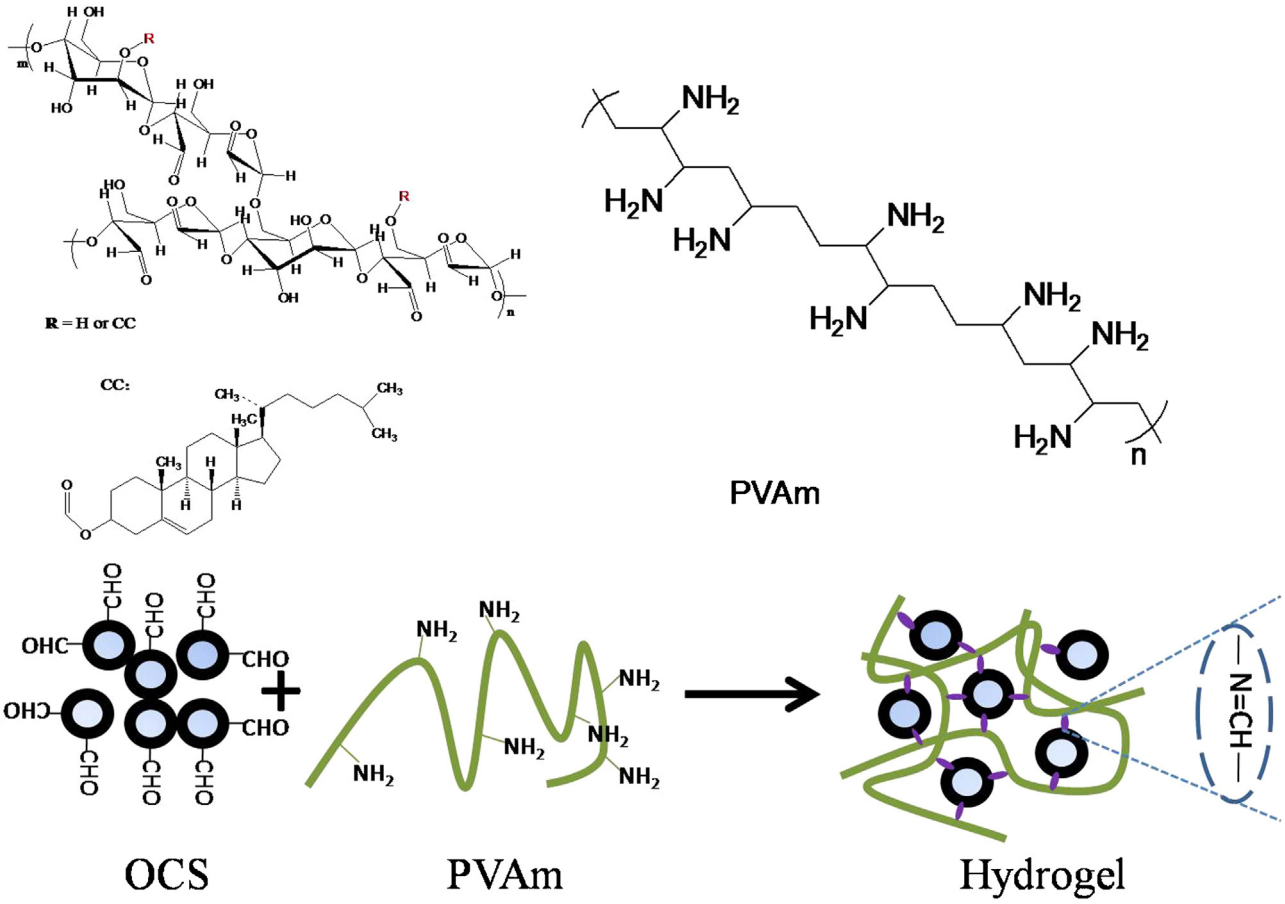

Fig. 1. The potential chemical structure of OCS and PVAm and the schematic description of hydrogel formation process.

amylopectin is a highly branched molecule, with α-(1–4)-linked D-glucose backbones and exhibits about 5% of α-(1–6)-linked branches. As the cheapest and entirely biodegradable biopolymer, starch-based hydrogels are of interesting and widely investigated for biomedical applications. Wohl-Bruhn et al. (2012) has been prepared a biodegradable hydrogel based on hydroxyethyl starch methacrylate. The hydrogel showed a sustained release of FITC-anti-human antibodies in vitro and FITC-lgG in vivo. Guilherme et al. (2012) also developed a brain-resembling superabsorbent hydrogel via UV-induced copolymerization-crosslinking of vinyl-modified starch with acrylic acid in the presence of Fe_3O_4. The obtained hydrogel presented a well magnetic response for albumin release.

Here, in situ hydrogel synthesized from starch-based nanoparticles and polyvinylamine (PVAm) via a Schiff base reaction. PVAm has attracted much industrial and academic interest in metal chelation (Tbal, Morcellet, Delporte, & Morcellet, 1992), liquid chromatography (Crini, Morin, & Morcellet, 1999), pollution cleanup (Geckeler, 2008) or biodegradable (Saito et al., 2007) fields because of its amounts of high reactive amino groups. In our process, starch was successively decorated with cholesterol group and aldehyde groups. This modification sustains a certain hydrophilic–hydrophobic balance for starch macromolecules so that nanoparticles with well-defined core–shell structure were obtained. The hydrogel was synthesized via a Schiff base reaction between the aldehyde groups of starch-based nanoparticles and the amine groups of PVAm (Fig. 1). The obtained hydrogel had good water capacity ability and well mechanical strength. DOX, as a model drug, was used to simulate its controlled-release behaviors.

2. Experiment

2.1. Materials

The corn starch was purchased from Changchun Dacheng Corn Development Co. Ltd. (China). The amylose and amylopectin content is 27% and 73%, respectively. Corn starch with macromolecular weight (*Mw*) of 200,000 Da was obtained according to a previously published method (Tan et al., 2009). Sodium periodate (AR), cholesteryl chloroformate (98%) and N-vinyformamide (96%) was purchased from Aladdin Chemistry Co., Ltd. Polyvinylamine (PVAm) was prepared from N-vinyformamide as reported (Gu, Zhu, & Hrymak, 2002). Doxorubicin hydrochloride (DOX) was purchased from Beijing Zhongshuo Pharmaceutical Technology Development Co., Ltd. All the other chemicals were obtained from Beijing Chemical Factory and used as received.

2.2. Synthesis of cholesterol based starch (CS)

In a typical procedure, starch (5.0 g) was carefully added to molten imidazole (50.0 g) at 100 °C under stirring. After 30 min a clear starch solution was obtained. Cholesteryl chloroformate (0.135 g, 0.01 mol/mol anhydroglucose unit, AGU) was added to the starch solution and allowed to react for 1 h at 100 °C under stirring. The product was precipitated, washed repeatedly with ethanol until filtrate free of imidazole as detected. The final product was dried at 50 °C in the oven.

The degree of the cholesterol substitution (DS_{ch}) determined by the integration of the area of the cholesterol to the AGU in

^{1}H NMR spectroscopy was 0.01. ^{1}H NMR (400 MHz, DMSO-d6) δ (ppm) = 2.0–0.5 (cholesterol H), 5.3–3.1 (AGU H).

2.3. Synthesis of the oxidative CS (OCS)

OCS was synthesized by periodate oxidation of CS as described earlier (Veelaert, de Wit, Gotlieb, & Verhe, 1997a,b) with some modifies. CS (3.0 g) was suspended in 20 mL distilled water in a three-necked flask. Then sodium periodate (1.96 g) was added into the suspension and the pH value was adjusted to 3.0 by adding 1% (w/v) hydrochloric acid. Then the mixture was mechanical stirred at the speed of 250 rpm, and incubated in a water bath at 37 °C, keep the reaction in the dark for 3 h. After that the sample was filtered and thoroughly washed with ethanol for five times. The obtained OCS was then dried in an oven at 50 °C.

The degree of oxidation determined by the repaid quantitative alkali consumption method (Hofreiter, Alexander, & Wolff, 1955) was 46%. ^{1}H NMR (400 MHz, DMSO-d6) δ (ppm) = 4.0–4.6 (hemiacetal –CH), 6.3–7.3 (hemiacetal –OH), 2.0–0.5 (cholesterol H), 5.3–3.1 (AGU H).

2.4. Preparation of the oxidative starch (OS)

As simply, the starch was processed as the description in Section 2.2 without the addition of cholesteryl chloroformate and oxidized as the description in Section 2.3. The degree of oxidation determined by the repaid quantitative alkali consumption method was 43%.

2.5. Preparation of the nanoparticles

Hundred milligram OCS was dissolved in 1 mL distil water in a vial with continuous stirring in 70 °C. About 10 min later, a homogeneous nanoparticle suspension was obtained. Then put it in refrigerator at 5 °C for further application.

2.6. Preparation of hydrogels

OCS and PVAm were firstly dissolved in water to form 10% solutions, and stored at 5 °C. The hydrogels were prepared by mixing of OCS and PVAm solutions with different volume ratio in syringes under shaking. The mixture was maintained at 25 °C sealed by parafilm for gelation.

2.7. Characterization

FTIR characterization was performed on Perkin-Elmer Spectrum 100 spectrometer (USA) using ATR model, and the data were collected via 32 scans with a resolution of 2 cm^{-1} at room temperature. ^{1}H NMR spectra were recorded using a Bruker AV400 spectrometer (Germany) operating at room temperature. All of the samples were dissolved in DMSO-d_6.

The appearance of nanoparticles was characterized by transmission electron microscopic (TEM, Hitachi H-800) observation at an acceleration voltage of 100 kV. The lyophilized hydrogel was characterized by scanning electron microscopy (SEM) with the accelerating voltage 10.0 kV using a Model XL 30 ESEM (Philips).

2.8. Rheological measurements

Rheological experiments were carried out on a PHYSICA MCR 300 instrument (Stuttgart, Germany). Frequency sweep for the samples was carried out at 25 °C using 25 mm plate–plate geometry. The strain γ and angular frequency range used during testing were 1% and 0.1–100 rad/s, with a normal force 0.5 N. MCR300 software was used to acquire data.

2.9. Swelling experiments

Completely cured cylindrical hydrogel sample was immersed into distil water or phosphate buffered saline (PBS pH = 7.4) solutions at 25 °C. At predetermined time points, the water or PBS solutions was removed and the gels were blotted and weighed. Fresh distil water or PBS solutions was added, and swelling continued until equilibrium, that is, no further change in weight with increasing time. The swelling degree (SW) was determined by the equation as follow (Chen, Xu, Feng, Wang, & Li, 2010).

$$SW = \left(\frac{M_t - M_0}{M_0}\right) \times 100\%$$

where M_0 represents the weight of the dry hydrogel, M_t represents the weights of the hydrogel at any time. All the experiments were carried out with three samples and the reported data were average values.

2.10. Release of DOX from hydrogel

For DOX release experiment, DOX was dissolved in PVAm solution to in situ form DOX-loaded hydrogel. Hydrogel samples were immersed into PBS (pH = 3.0, 5.0, 7.4), sealed in a dialysis bag (*Mw* cutoff: 3.5 kDa) and incubated in the release medium containing 0.05 g/L sodium azide (25 mL) at 37 °C under oscillation at 45 rpm. At selected time intervals, buffer solution outside the dialysis bag was removed for UV–vis analysis and replaced with fresh buffer solution. The released amount of DOX was determined from the absorbance at 480 nm with the help of a calibration curve of DOX in the same buffer. Then the accumulative weight and relative percentage of the released DOX were calculated as a function of incubation time.

3. Results and discussion

3.1. Synthesis and characterization of OCS and OS

In our approach, starch was firstly etherized using cholesteryl chloroformate in a green media of imidazole. The molten imidazole could completely dissolve starch to provide a homogeneous reaction conditions. More important, imidazole also acted as reagent and base to made the reaction system very simple, efficient and economically attractive when starch reacted with acid chloride, by which imidazolide was in situ formed firstly and reacted with starch to yields products with a very high purity (Liebert et al., 2011).

The degree of cholesterol substitution on starch could be controlled by the amount of cholesteryl chloroformate which was fed in the reaction. The structural feature of CS was characterized by ^{1}H NMR spectroscopy. As shown in Fig. 2A(B), the character peaks of cholesterol at 0.5–2.0 ppm could be observed (Filippov et al., 2012). It confirmed that the cholesterol group was successfully grafted on the backbone of the starch. It was noted that the DS_{ch} (the degree of cholesterol substitution) could not beyond 0.01. Otherwise, after oxidation the nanoparticles could not disperse uniformly in aqueous.

The CS was then oxidized by sodium periodate in water. This oxidation process afforded starch-based macromolecules aldehyde group. As shown in Fig. 2A(C and D), some new peaks ranges from 4.0 ppm to 4.6 ppm and from 6.3 ppm to 7.3 ppm were appeared. These new peaks were attributed to the hemiacetals groups. Generally, the proton peak of the aldehyde was on the region of from 9.0 ppm to 10 ppm. However, such peak was so weak at 9.3 ppm. This fact could be explained that aldehyde exhibited equilibrium

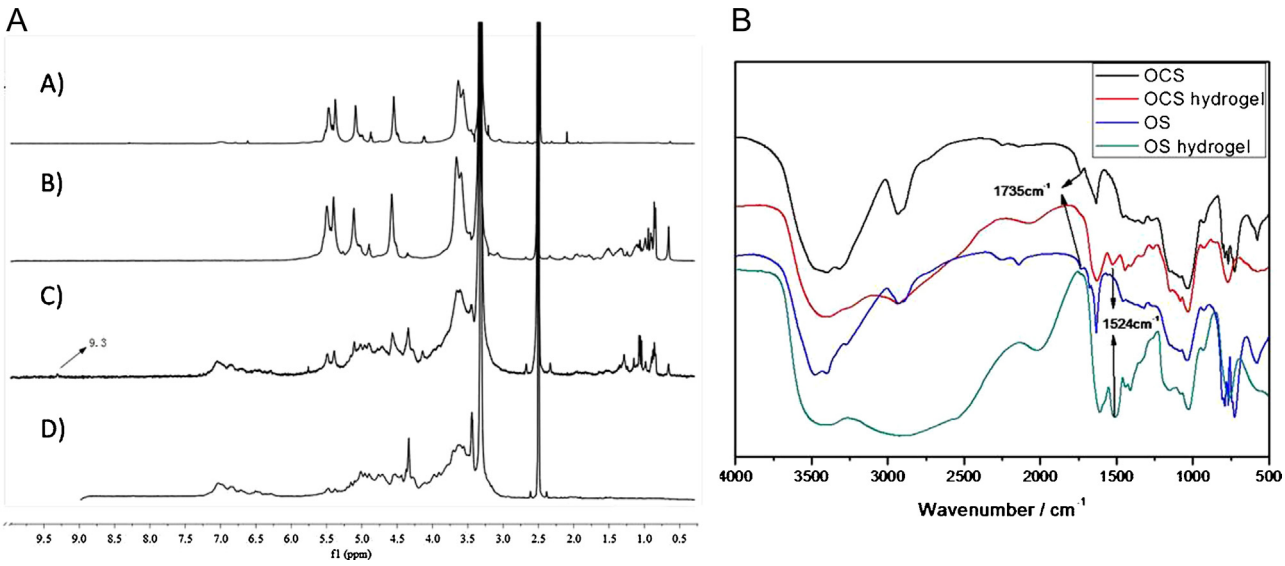

Fig. 2. (A) ^{1}H NMR (400 MHz) spectra of (A) starch, (B) CS, (C) OCS and (D) OS in DMSO-d_6; (B) The FTIR of the OCS/OS and the dry hydrogel (OCS(OS)/PVAm = 1:1) respectively.

with hemiacetals (reaction between an aldehyde and a hydroxyl or reaction between two aldehyde moieties) (Serrero et al., 2010). So we attributed these two peaks as the protons of methylene groups and the protons of hydroxyl groups on the hemiacetals, respectively.

3.2. Preparation of nanoparticles

The nanoparticles were formed by dispersion the OCS in water at 70 °C for 10 min. After complete dispersion, the particle size analyzer (PSA) measurement indicated that nanoparticles exhibited mean size and polydispersity index of ~143 nm and 0.127, respectively (insert of Fig. 3A). Moreover, TEM characterization indicated that OCS nanoparticles exhibited well-defined core–shell structure (Fig. 3A), while no nanoparticle could be observed in OS solution (Fig. 3B). It could be explained that the hydrophobic cholesterol groups in the backbone of starch was aggregated to form the core, while the hydrophilic aldehyde groups aggregated at the surface of nanoparticles. Moreover, this fact could be confirmed that the shell of few nanoparticles was darker than the core because of staining by trace of iodine, which was very hard to be cleared after oxidation by sodium periodate (Veelaert et al., 1997a,b). Therefore, we could conclude that the shell was mainly composed of derivable aldehyde groups, facilitating the further reaction with other functional groups.

3.3. Preparation of hydrogels

After mixing the PVAm and OCS/OS solution, the hydrogel could be formed in situ crosslinked via Schiff base reactions between amine and aldehyde groups. The structure of hydrogels was confirmed by FTIR characterization depicted in Fig. 2B, the peak of aldehyde groups of OCS/OS in the wave-number 1732 cm^{-1} was decreased and became a shoulder after reaction. In addition, although the character peak for imine in 1665 cm^{-1} might be masked by the multiple absorbance peaks at this wave-number, a new peak around 1524 cm^{-1} is presented. Presumably it is the character peak of amino group. These facts indicated the occurrence of the Schiff base reactions.

3.4. Rheological analysis

For in situ formed hydrogel, rheological experiment is most powerful approach to quantitatively characterize its gelatin process. Fig. 4A presents the temporal variation of the storage modulus (G') and the loss modulus (G'') of OCS/PVAm hydrogel (OCS hydrogel

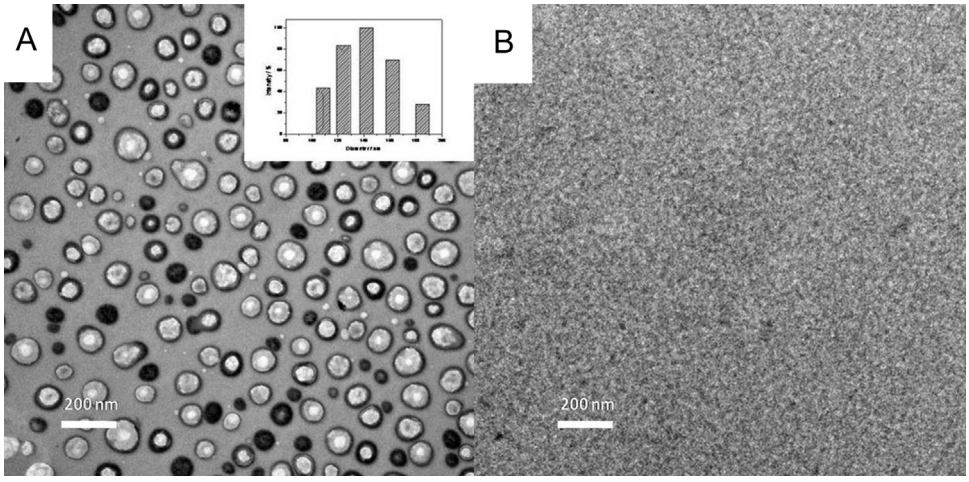

Fig. 3. (A) The TEM image of OCS nanoparticles (insert the particle size distribution obtained by DLS characterization) and (B) the TEM image of OS.

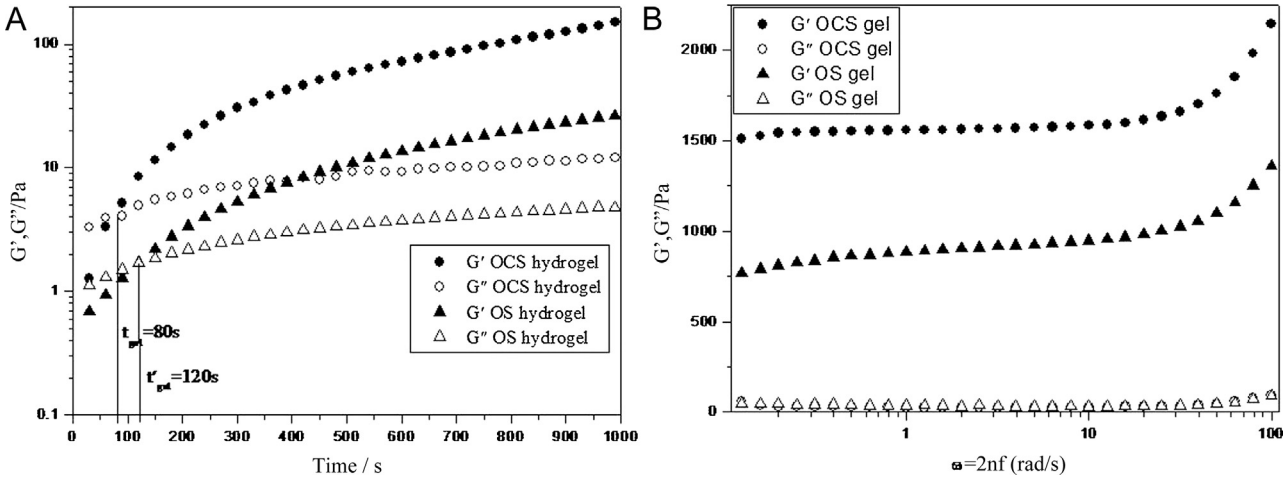

Fig. 4. (A) Time evolution of the storage modulus (G') and the loss modulus (G'') of (A) OCS hydrogel (simple 4) and (B) OS hydrogel (simple 9) formed by self-cross-linking. G' and G'' crossover is denoted as t_{gel} (gelation point); (B) The modulus' contrast of OS based hydrogel and the OCS based hydrogel when the $-NH_2/-CHO$ (v/v) = 1/1. All solutions were adjusted to pH = 1.5, with concentration of 10 wt%.

which was represent the hydrogel formed by simple 4 in Table 1) and OS/PVAm hydrogel (OS hydrogel which was represent the hydrogel formed by simple 9 in Table 1), which had equal concentration (10 wt%) and volume ratio (1:1). It was found that the G' was increased faster than G'' due to the formation of cross-linking network. The different elevation rates of G' and G'' led to a crossover ($t = t_{gel}$, where t_{gel} was the gel point) (Zhang, Qadeer, Mynarcik, & Chen, 2011), indicating the transition of the precursor from a liquid phase to a solid phase. We could conclude that OCS hydrogel exhibits a t_{gel} of 80 s, while OS hydrogel exhibited a slower t_{gel} of 120 s. Both the gel point times were at the same level. This fast gelation of OCS hydrogel possibly resulted from the peculiar microstructure of OCS, by which the derivable aldehyde groups situated at the surface of nanoparticles. This implied that the shell was mainly composed of derivable aldehyde groups, facilitating the further reaction with other functional groups. It was noted that both G' continued to elevate during the entire time span of testing. This indicated both reactions continued and the modulus continued to increase until a well-developed 3D network formation.

The relationships between the rheological properties and the aldehyde content of OCS were investigated; the results are summarized in Table 1. The rheological properties of the hydrogels formulated with different OCS/PVAm (the volume ratio of the two components maintained at unity) were evidently different, indicating that the aldehyde content in OCS was a key factor to the hydrogels' rheological properties. It could be deduced that both the gelation time and mechanical properties of the hydrogel could be modulated by changing the aldehyde content of OCS; either excessive or insufficient amounts of aldehyde groups on the OCS adversely affected the cross-linking reaction of the two components. When the volume ratio of OCS/PVAm = 1/1, the mixed precursor showed the highest mechanical strength (G' = 1530 Pa) and the shorter gelation time (80 s). Hypothetically, this formulation could give enough time for material preparation and rapid gelation if an injectable formulation was to be contemplated.

Table 1
the characteristics of hydrogels formed with different volume ratio between OCS solutions (10 wt%) and PVAm solutions (10 wt%) at 25 °C. The sol and gel represents solution and hydrogel, respectively.

Sample	PVAm/OCS (v/v)	t_{gel} (s)	Product[a]	Modulus[b] (Pa)
1	8/1		Sol	
2	4/1	264	Gel	208
3	2/1	160	Gel	800
4	1/1	80	Gel	1530
5	1/2	120	Gel	1262
6	1/4	148	Gel	934
7	1/8	220	Gel	317
8	1/16		Sol	
9[c]	1/1	120	Gel	980

[a] Product is the appearance of the system.
[b] Modulus is the max mechanical strength of the hydrogel.
[c] OS is used to synthesize hydrogel.

After incubated in 37 °C for 24 h, the well defined hydrogel' modulus (G' and G'') were tested. As shown in Fig. 4B, both at low and high frequency, the OCS based gel exhibited high modulus compared to OS based gel. So it is evidenced that the introduction of the hydrophobic cholesterol group could improve the modulus of the hydrogel to some extent. This is because the OCS nanoparticles acted as nanoscale crosslinking points evenly distributed in the whole hydrogel network, and the flexible polymer chains between the nanoparticles share approximately similar chain length, so the stress can be easily dissipated by hydrogels. Based on this hypothesis, a schematic illustration of hydrogel network structure is shown in Fig. 1, where the polymer chains pass though the starch based nanoparticles.

In addition, it was noted that some unusual curves were appeared at high frequency area. For ideal gel, the storage modulus (G') should exhibit a pronounced plateau extending to times at least on the order of seconds in this region. At the low frequency, the hydrogels showed a plateau from 0.01 rad/s to 10 rad/s, which was the character of an ideal gel. While at the high frequency, the storage modulus (G') was increasing with the frequency increasing. That phenomenon could be explained as follow: the short polymer chains in a cross-linking network can be adjusted itself in a short time, so they have a smaller relaxation times (Liu, Li, Rong, & Zhou, 2012; Moura, Figueiredo, & Gil, 2007; Skelton et al., 2013). While both of the OCS/OS and PVAm were macromolecular that have long polymer chains, the cross-linking density was low. So the cross-linking network was loose. When the loosely cross-linking network was exposed in high frequency, it could not rearrange themselves because of the long chains. So they became stiff just as a solid-like behavior. That could be showed by an increase in G'.

3.5. Morphology of OCS/OS hydrogels

Generally, the micro-structure of the materials played an important role to improve the mechanical properties of the polymer. So it was necessary to investigate the micro-structure of the

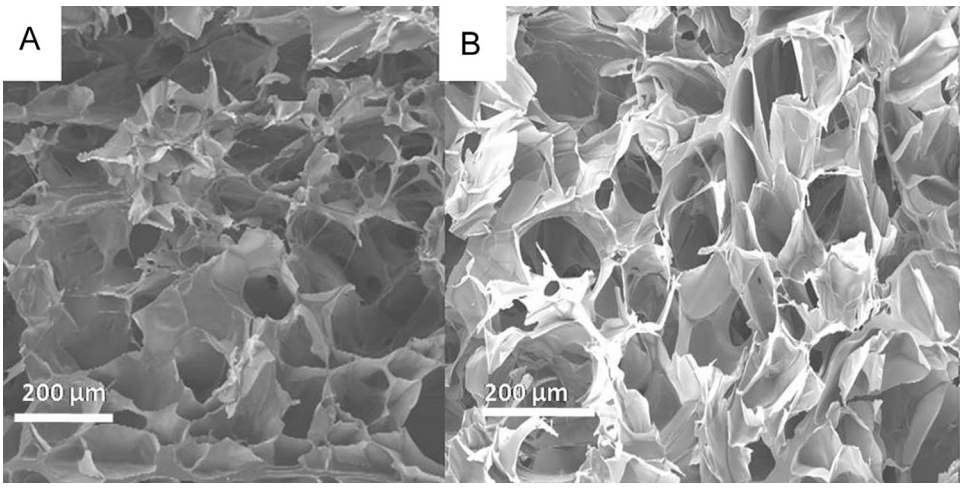

Fig. 5. The SEM of OS (A, sample 9) and OCS (B, sample 4) based hydrogel.

hydrogel. The cross-sectional SEM of lyophilized OCS/OS based hydrogels is depicted in Fig. 5. Although both hydrogels had porous interior structures with interconnected pores, their pore size distributions and the thick of the matrix from surrounding pores were obviously different. The OCS based hydrogel had well-defined pore size (~150 μm) and thicker matrix compared with OS based hydrogel. The thicker matrix could hold larger energy when it met force. That would contribute to higher mechanical strength for OCS based hydrogel.

3.6. Swelling analysis

Hydrogels are three dimensional hydrophilic polymeric networks that absorb and retain water or biological fluids in their structure. The swelling of polymer chains reached equilibrium at a point where the swelling force was just balanced by the elastic restoring force acting in the opposite direction. Here, the swelling equilibrium of the OCS and OS based hydrogel were investigated. As shown in Fig. 6A, the swelling equilibrium for both hydrogel could be reached within 500 s. The OCS hydrogel absorbed 18.4 times water while OS hydrogel absorbed about 8.2 times water. Moreover, the swelling process of both hydrogels could be differentiated at two stages. At first 25 s, the rate of water capacity was almost similarly for both hydrogels. This stage was the result of water absorption for the surface of the hydrogels. When the water on the surface of the hydrogel was getting saturation, its absorbed rate was decreased remarkably. Notably, the OCS hydrogel exhibited a faster adsorption than OS hydrogel. This stage could be attributed to the penetrating of water into the inside of the hydrogel, by which the pore diameter and distribution might play an important role. As had been reported by (Tanaka, Sato, Hirokawa, Hirotsu, & Peetermans, 1985); for the water diffusion of the hydrogel, the pore diameter was inversely proportional to the friction. If the friction was big, the diffusions speed of water would be slow down. For OS and OCS hydrogel, although both of the dry hydrogels were porous, the average diameters were 100 μm and 150 μm respectively. So when the water penetrated into the gel, the OS hydrogel met bigger friction. As a result, the diffusions speed for OCS hydrogel was bigger than the OS hydrogel. So the rate of water capacity for OCS hydrogel was faster than the OS hydrogel. Otherwise, OCS hydrogel had bigger pore size, so it could absorb more water. The high void ratio made the gel easy to absorb water from the environment around in a short time.

We also investigated the swelling degree of the hydrogels in PBS solutions with different pH value. As shown in Fig. 6B, with the pH value increasing, the swelling degree of the hydrogel was increasing overall. This fact could be explained by the electrostatic interactions. At low pH value, the gel which containing amounts of unreacted amino groups got shrank in the presence of a large number of cations. So the water contained ability was low. With the

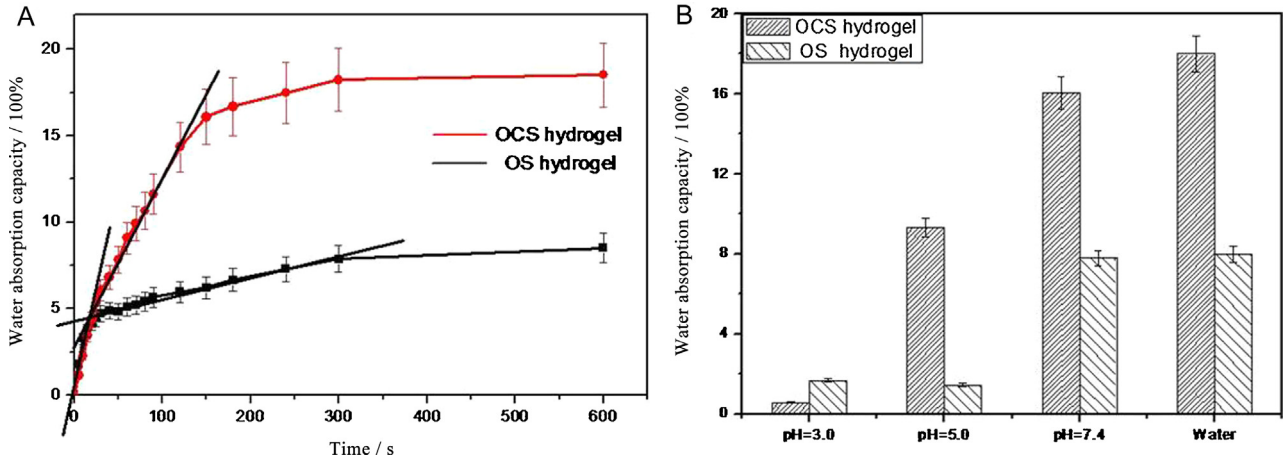

Fig. 6. (A) Water capacity ability of the OS hydrogel (simple 9) and OCS hydrogel (simple 4) in distil water; (B) water absorption capacity of the OS hydrogel (simple 9) and OCS hydrogel (simple 4) in various PBS solutions or water.

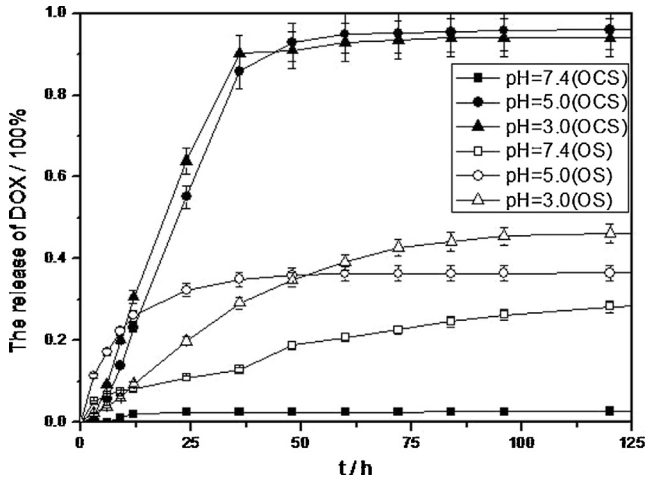

Fig. 7. Effect of pH on DOX release from OCS/OS hydrogels. hydrogel: (PVAm: OCS(OS) = 1:1, v/v), media: PBS(pH 7.4), 0.05 M NaH_2PO_4 + 0.15 M NaCl ± H_3PO_4 (pH 5.0), 0.05 M NaH_2PO_4 + 0.15 M NaCl ± H_3PO_4 (pH 3.0).

pH increasing, the gel got swelling as a result of the reducing of the cations in solutions. While the OCS hydrogel had an obvious change compared with the OS hydrogel. The phenomenon may be with the relationship to the structure of the hydrogel. The OCS hydrogel had a regular shape, so it could absorb large amounts of water. While for the OS hydrogel, it could not absorb water uniformly.

3.7. Release of DOX

Based on the 3D structure of hydrogels, it was a suitable material to transmit the target drug to the right place. Here, DOX was used as model drug to investigate the control and release properties of OCS hydrogels. The DOX release from the drug-loaded hydrogels was studied in PBS buffer with pH of 3.0, 5.0 and 7.4, respectively. As shown in Fig. 7, there was no dramatic initial burst release for drug-loaded OCS hydrogels at different pH value. However, the hydrogels present a pH-sensitive released profiles. The lower the pH value, the faster the drug was released. The OCS hydrogel showed sustained release of DOX at pH = 7.4, only 3% was released in 36 h. In the same time period, it released 85.9% of DOX at pH = 5.0 and 90.3% at pH = 3.0. However, for the OS hydrogel, although the released DOX was higher in pH = 7.4 compared with the OCS hydrogel, at lower pH the amount of released DOX was not more than 50% after 100 h later.

These results could be explained by the hydrolysis of the Schiff base reaction between the amino group of the DOX and the aldehyde of OS/OCS and the uniform of the pore size of the hydrogel. The imine group was fragile at acid condition and the stability of these bonds decreases as the pH decreases. It was noted that the release rate was very low at first 3 h, which was mainly due to the penetration of water into the hydrogel networks. At same acid condition, the dispersion of the pore might play an important role. The well dispersed pore could easily spread the drug out of the hydrogel. So the OCS hydrogel had a better release behavior.

Therefore, the drug-loaded hydrogels prefer to release in an acid environment, and damage normal cells and tissues could be avoided. These released properties of OCS hydrogels were highly desirable for effective treatment of cancer, since tumor tissues were known to be acidic.

4. Conclusion

We demonstrated a robust method to synthesize in situ hydrogel base on natural polysaccharides derivates. It was found that the OCS shows well defined core–shell nanoparticles in aqueous, by which the derivable aldehyde groups distributed on the shell of nanoparticles facilitating its further reaction with other functional groups. The starch-based nanoparticles and polyvinylamine in situ cross-linked to form hydrogels via a Schiff base reaction. The OCS hydrogels have better strength compared the OS hydrogels. And the dried OCS hydrogels have well dispersion pore structure compared with the OS hydrogels. The degree of swelling of the hydrogel in various PBS solutions was increasing with the pH values increasing. Moreover, we used DOX as a model drug to simulate the controlled-release properties of OCS hydrogels. The result showed that DOX-loaded OCS hydrogels prefer to release in an acid environment. Its released properties are highly desirable for effective treatment of cancer. Further study will focus on the biodegradable properties and in vivo cytotoxic experiments of OCS hydrogels.

Acknowledgement

Financial support from the National Natural Science Foundation of China (grant nos. 51321062 and 51103150) is gratefully acknowledged.

References

Boucard, N., Viton, C., & Domard, A. (2005). New aspects of the formation of physical hydrogels of chitosan in a hydroalcoholic medium. *Biomacromolecules*, *6*(6), 3227–3237.

Censi, R., Fieten, P. J., di Martino, P., Hennink, W. E., & Vermonden, T. (2010). In situ forming hydrogels by tandem thermal gelling and michael addition reaction between thermosensitive triblock copolymers and thiolated hyaluronan. *Macromolecules*, *43*(13), 5771–5778.

Chen, X., Xu, S., Feng, S., Wang, J., & Li, X. (2010). Preparation and swelling behavior of pH-sensitive and salt-resistant amphoteric semi-IPNs hydrogels based on starch phosphate and poly 2-(methacryloyloxy) ethyl trimethylammonium chloride. *E-Polymers*, *10*(1), 1203–1213.

Chiu, Y.-L., Chen, S.-C., Su, C.-J., Hsiao, C.-W., Chen, Y.-M., Chen, H.-L., et al. (2009). pH-triggered injectable hydrogels prepared from aqueous N-palmitoyl chitosan: In vitro characteristics and in vivo biocompatibility. *Biomaterials*, *30*(28), 4877–4888.

Crini, G., Morin, N., & Morcellet, M. (1999). High-performance liquid chromatography of structural isomers with cyclodextrin-poly(vinylamine)-coated silica columns, part III: Retention mechanism study of nitrophenol derivatives. *Journal of Chromatographic Science*, *37*(4), 121–125.

Ding, B., Cai, J., Huang, J., Zhang, L., Chen, Y., Shi, X., et al. (2012). Facile preparation of robust and biocompatible chitin aerogels. *Journal of Materials Chemistry*, *22*(12), 5801–5809.

Fan, Y., Deng, C., Cheng, R., Meng, F., & Zhong, Z. (2013). In situ forming hydrogels via catalyst-free and bioorthogonal "tetrazole–alkene" photo-click chemistry. *Biomacromolecules*, *14*(8), 2814–2821.

Filippov, S. K., Chytil, P., Konarev, P. V., Dyakonova, M., Papadakis, C. M., Zhigunov, A., et al. (2012). Macromolecular HPMA-based nanoparticles with cholesterol for solid-tumor targeting: Detailed study of the inner structure of a highly efficient drug delivery system. *Biomacromolecules*, *13*(8), 2594–2604.

Geckeler, K. (2008). Water-based metal remediation processes: Basics and novel developments. In P. Tundo, & V. Esposito (Eds.), *Green chemical reactions* (pp. 131–153). Netherlands: Springer.

Gu, L., Zhu, S., & Hrymak, A. N. (2002). Acidic and basic hydrolysis of poly(N-vinylformamide). *Journal of Applied Polymer Science*, *86*(13), 3412–3419.

Guilherme, M. R., Oliveira, R. S., Mauricio, M. R., Cellet, T. S. P., Pereira, G. M., Kunita, M. H., et al. (2012). Albumin release from a brain-resembling superabsorbent magnetic hydrogel based on starch. *Soft Matter*, *8*(24), 6629–6637.

Hofreiter, B. T., Alexander, B. H., & Wolff, I. A. (1955). Rapid estimation of dialdehyde content of periodate oxystarch through quantitative alkali consumption. *Analytical Chemistry*, *27*(12), 1930–1931.

Kiyonaka, S., Sada, K., Yoshimura, I., Shinkai, S., Kato, N., & Hamachi, I. (2004). Semi-wet peptide/protein array using supramolecular hydrogel. *Nature Materials*, *3*(1), 58–64.

Li, C., & Mezzenga, R. (2012). Functionalization of multiwalled carbon nanotubes and their pH-responsive hydrogels with amyloid fibrils. *Langmuir*, *28*(27), 10142–10146.

Liebert, T., Nagel, M. C. V., Jordan, T., Heft, A., Grünler, B., & Heinze, T. (2011). Pure, transparent-melting starch esters: Synthesis and characterization. *Macromolecular Rapid Communications*, *32*(17), 1312–1318.

Liu, M., Li, W., Rong, J., & Zhou, C. (2012). Novel polymer nanocomposite hydrogel with natural clay nanotubes. *Colloid and Polymer Science*, *290*(10), 895–905.

Moura, M. J., Figueiredo, M. M., & Gil, M. H. (2007). Rheological study of genipin cross-linked chitosan hydrogels. *Biomacromolecules*, *8*(12), 3823–3829.

Nair, S., Remya, N. S., Remya, S., & Nair, P. D. (2011). A biodegradable in situ injectable hydrogel based on chitosan and oxidized hyaluronic acid for tissue engineering applications. *Carbohydrate Polymers*, *85*(4), 838–844.

Nowak, A. P., Breedveld, V., Pakstis, L., Ozbas, B., Pine, D. J., Pochan, D., & Deming, T. J. (2002). Rapidly recovering hydrogel scaffolds from self-assembling diblock copolypeptide amphiphiles. *Nature*, *417*(6887), 424–428.

Palumbo, F. S., Pitarresi, G., Fiorica, C., Matricardi, P., Albanese, A., & Giammona, G. (2012). In situ forming hydrogels of new amino hyaluronic acid/benzoyl-cysteine derivatives as potential scaffolds for cartilage regeneration. *Soft Matter*, *8*(18), 4918–4927.

Park, S.-A., Jang, E., Koh, W.-G., & Kim, B. (2010). Fabrication and characterization of optical biosensors using polymer hydrogel microparticles and enzyme-quantum dot conjugates. *Sensors and Actuators B-Chemical*, *150*(1), 120–125.

Peng, G., Wang, J., Yang, F., Zhang, S., Hou, J., Xing, W., et al. (2013). In situ formation of biodegradable dextran-based hydrogel via Michael addition. *Journal of Applied Polymer Science*, *127*(1), 577–584.

Qiu, Y., & Park, K. (2012). Environment-sensitive hydrogels for drug delivery. *Advanced Drug Delivery Reviews*, *64*(Supplement (0)), 49–60.

Saito, H., Hoffman, A. S., & Ogawa, H. I. (2007). Delivery of doxorubicin from biodegradable PEG hydrogels having Schiff base linkages. *Journal of Bioactive and Compatible Polymers*, *22*(6), 589–601.

Serrero, A., Trombotto, S., Cassagnau, P., Bayon, Y., Gravagna, P., Montanari, S., et al. (2010). Polysaccharide gels based on chitosan and modified starch: Structural characterization and linear viscoelastic behavior. *Biomacromolecules*, *11*(6), 1534–1543.

Seliktar, D. (2012). Designing cell-compatible hydrogels for biomedical applications. *Science*, *336*(6085), 1124–1128.

Skelton, S., Bostwick, M., O'Connor, K., Konst, S., Casey, S., & Lee, B. P. (2013). Biomimetic adhesive containing nanocomposite hydrogel with enhanced materials properties. *Soft Matter*, *9*(14), 3825–3833.

Sugaya, S., Kakegawa, S., Fukushima, S., Yamada, M., & Seki, M. (2012). Micropatterning of hydrogels on locally hydrophilized regions on PDMS by stepwise solution dipping and in situ gelation. *Langmuir*, *28*(39), 14073–14080.

Tan, Y., Wang, P., Xu, K., Li, W., An, H., Li, L., et al. (2009). Designing starch-based nanospheres to make hydrogels with high mechanical strength. *Macromolecular Materials and Engineering*, *294*(12), 855–859.

Tanaka, T., Sato, E., Hirokawa, Y., Hirotsu, S., & Peetermans, J. (1985). Critical kinetics of volume phase transition of gels. *Physical Review Letters*, *55*(22), 2455–2458.

Tbal, H., Morcellet, J., Delporte, M., & Morcellet, M. (1992). Uranium adsorption by chelating resins containing amino groups. *Journal of Macromolecular Science Part A*, *29*(8), 699–710.

Tokarev, I., & Minko, S. (2010). Stimuli-responsive porous hydrogels at interfaces for molecular filtration, separation, controlled release, and gating in capsules and membranes. *Advanced Materials*, *22*(31), 3446–3462.

Van Tomme, S. R., van Steenbergen, M. J., De Smedt, S. C., van Nostrum, C. F., & Hennink, W. E. (2005). Self-gelling hydrogels based on oppositely charged dextran microspheres. *Biomaterials*, *26*(14), 2129–2135.

Veelaert, S., de Wit, D., Gotlieb, K. F., & Verhe, R. (1997). Chemical and physical transitions of periodate oxidized potato starch in water. *Carbohydrate Polymers*, *33*(2–3), 153–162.

Veelaert, S., deWit, D., Gotlieb, K. F., & Verhe, R. (1997). The gelation of dialdehyde starch. *Carbohydrate Polymers*, *32*(2), 131–139.

Wang, J., Zong, J.-Y., Zhao, D., Zhuo, R.-X., & Cheng, S.-X. (2011). In situ formation of chitosan-cyclodextrin nanospheres for drug delivery. *Colloids and Surfaces B: Biointerfaces*, *87*(1), 198–202.

Wang, A., Cui, Y., Li, J., & van Hest, J. C. M. (2012). Fabrication of gelatin microgels by a cast strategy for controlled drug release. *Advanced Functional Materials*, *22*(13), 2673–2681.

Weng, L., Rostambeigi, N., Zantek, N. D., Rostamzadeh, P., Bravo, M., Carey, J., et al. (2013). An in situ forming biodegradable hydrogel-based embolic agent for interventional therapies. *Acta Biomaterialia*, *9*(9), 8182–8191.

Wohl-Bruhn, S., Badar, M., Bertz, A., Tiersch, B., Koetz, J., Menzel, H., et al. (2012). Comparison of in vitro and in vivo protein release from hydrogel systems. *Journal of Controlled Release: Official Journal of the Controlled Release Society*, *162*(1), 127–133.

Yang, Y., & Urban, M. W. (2013). Self-healing polymeric materials. *Chemical Society Reviews*, *42*, 7446–7467.

Yu, F., Cao, X., Li, Y., Zeng, L., Yuan, B., & Chen, X. (2014). An injectable hyaluronic acid/PEG hydrogel for cartilage tissue engineering formed by integrating enzymatic crosslinking and Diels–Alder "click chemistry". *Polymer Chemistry*, *5*(3), 1082–1090.

Zhang, H., Qadeer, A., & Chen, W. (2011). In situ gelable interpenetrating double network hydrogel formulated from binary components: Thiolated chitosan and oxidized dextran. *Biomacromolecules*, *12*(5), 1428–1437.

Zhang, H., Qadeer, A., Mynarcik, D., & Chen, W. (2011). Delivery of rosiglitazone from an injectable triple interpenetrating network hydrogel composed of naturally derived materials. *Biomaterials*, *32*(3), 890–898.